

¹ **Mediterranean drought variability over the last millennium**

Benjamin I Cook^{1,2}, Kevin J Anchukaitis³, Ramzi Touchan⁴, David M Meko⁴,

and Edward R Cook⁵

Corresponding author: Benjamin I Cook, NASA Goddard Institute for Space Studies, New York, New York, USA. (benjamin.i.cook@nasa.gov)

¹NASA Goddard Institute for Space Studies, New York, New York, USA.

²Ocean and Climate Physics,
Lamont-Doherty Earth Observatory,
Palisades, New York, USA.

³Woods Hole Oceanographic Institution,
Woods Hole, Massachusetts, USA.

⁴Laboratory of Tree-Ring Research,
University of Arizona, Tucson, Arizona,
USA.

⁵Tree Ring Laboratory, Lamont-Doherty
Earth Observatory, Palisades, New York,
USA.

Abstract. Recent droughts in the Mediterranean have highlighted concerns that climate change may be contributing to recent drying trends, but the full range of natural climate variability in the region is still poorly understood. Here, we analyze 900 years (1100–2012) of Mediterranean drought variability in the Old World Drought Atlas (OWDA), a spatiotemporal tree-ring based reconstruction of the June–July–August self calibrating Palmer Drought Severity Index. In the Mediterranean, the OWDA is highly correlated with spring precipitation (April–June) and the North Atlantic Oscillation (January–April), the Scandinavian Pattern (January–March), and the East Atlantic Pattern (April–June). Drought variability in the basin shows significant east-west coherence on multi-decadal to centennial time scales. There is also an apparent North-South dipole in the eastern Mediterranean, with a tendency for Greece and Anatolia to be wet when the southern Levant and coastal Libya and Egypt are dry, possibly related to variability in the North Atlantic Oscillation. Major droughts and drying trends over the last several decades are centered in the western Mediterranean, Greece, and the Levant region. Droughts of similar magnitudes in the western Mediterranean and Greece are apparent in the OWDA back to 1100 CE, but the most recent 15-year drought in the Levant (1998–2012) appears as the driest such period on the record. Estimating sampling uncertainties using a Monte-Carlo approach, we conclude that there is an 89% likelihood that the recent Levant drought is drier than any comparable period of the last 900 years, possibly indicating the emergence of a greenhouse gas forced drying signal.

1. Introduction

26 Climate change impacts on water resources are a significant concern in the regions sur-
27 rounding the Mediterranean Sea [*Iglesias et al.*, 2007; *García-Ruiz et al.*, 2011], an area
28 including southern Europe, Northern Africa, and the Levant (Cyprus, Israel, Jordan,
29 Lebanon, Palestine, Syria, Turkey) region of the Middle East. Projections from climate
30 models almost uniformly point towards drying in the Mediterranean from increased green-
31 house gas forcing in the coming decades [*Giorgi and Lionello*, 2008; *Seager et al.*, 2014],
32 part of an overall trend towards desiccation and poleward expansion of subtropical dry
33 zones [*Held and Soden*, 2006; *Seager et al.*, 2010]. Indeed, analyses of recent climate trends
34 in the region suggest that this process may have already begun [*García-Ruiz et al.*, 2011;
35 *Gleick*, 2014; *Hoerling et al.*, 2012; *Kelley et al.*, 2012, 2015].

36 However, a more complete understanding of natural Mediterranean drought variability
37 and anthropogenic moisture trends requires comparisons with longer term variability than
38 is observable from relatively short instrumental records. To this end, the paleoclimate
39 community has been active throughout this region, developing estimates of Common Era
40 drought variability from a variety of proxies, including tree-rings [*Choukri et al.*, 1995;
41 *Glueck and Stockton*, 2001; *Touchan et al.*, 2003; *Akkemik and Aras*, 2005; *Touchan et al.*,
42 2005; *Esper et al.*, 2007; *Andreu et al.*, 2007; *Nicault et al.*, 2008; *Touchan et al.*, 2008a;
43 *Büntgen et al.*, 2010; *Touchan et al.*, 2011; *Köse et al.*, 2011; *Touchan et al.*, 2014a],
44 sediment cores [e.g., *Jones et al.*, 2006; *Roberts et al.*, 2012; *Moreno et al.*, 2012], and
45 speleothems [e.g., *Jex et al.*, 2011; *Wassenburg et al.*, 2013]. To date, however, there is
46 little consensus across these different records regarding the character and dominant drivers

of drought variability across the basin over the last millennium. In particular, there are extant uncertainties regarding how widespread droughts are in the Mediterranean [Roberts *et al.*, 2012], the magnitude and timing of long-term trends and centennial-scale variability [Esper *et al.*, 2007; Touchan *et al.*, 2011; Wassenburg *et al.*, 2013], and how seasonal signals and large-scale climate modes are reflected in proxy reconstructions [Touchan *et al.*, 2014a, b; Seim *et al.*, 2014].

Given these uncertainties, the development and analyses of new large-scale reconstructions is imperative for improving our understanding of regional climate dynamics in the Mediterranean region. Here, we use a spatially resolved tree-ring based field reconstruction of European and Mediterranean drought to investigate the dominant spatial and temporal patterns of drought variability across the basin over the last millennium. Specifically, our analysis addresses three primary research questions: 1) What are the dominant modes of hydroclimate variability in the Mediterranean? 2) How spatially coherent are drought events across the Mediterranean basin? and 3) How do major recent droughts compare to long-term hydroclimate variability over the last millennium?

2. Materials and Methods

2.1. The Old World Drought Atlas

The Old World Drought Atlas [OWDA; Cook *et al.*, in review] is a new, tree-ring based reconstruction of summer season (June-July-August, JJA) self calibrating Palmer Drought Severity Index (scPDSI) [van der Schrier *et al.*, 2013]. The OWDA uses 106 tree-ring chronologies to reconstruct scPDSI at 5,414 half degree grid points for the entire Common Era over the European-Mediterranean domain (27°N – 71°N , 12°W – 45°E). The reconstruction uses the point-by-point method (ref XXXX) with a search radius of 1000

68 kilometers, meaning any grid cell can be reconstructed from proxy predictor series within
69 1000 kilometers. Proxy site locations in the Mediterranean portion of the OWDA (30°N –
70 47°N , 10°W – 45°E) are shown in Figure 1, along with the approximate start date of the
71 various records. We restrict our analysis to 1100–2012 CE, the interval during which the
72 Mediterranean domain is reasonably well covered by proxy sites. Values in the OWDA
73 up through 1978 are tree-ring reconstructed; from 1979–2012 the OWDA incorporates the
74 instrumental scPDSI.

75 The scPDSI is a modification of the original PDSI formulation of *Palmer* [1965], a
76 locally normalized drought index incorporating changes in supply (precipitation), de-
77 mand (evapotranspiration) and storage (soil moisture). PDSI has an inherent memory
78 timescale of 12–18 months [*Guttman*, 1998; *Vicente-Serrano et al.*, 2010], allowing the
79 JJA target of the OWDA to incorporate climate information from the previous winter
80 and spring, the main seasons of moisture supply to the Mediterranean. The scPDSI used
81 as the target for the OWDA reconstruction is based on the latest version (TS3.21) of the
82 high-resolution CRU gridded product [*Harris et al.*, 2014], incorporates a snow module,
83 and uses the Penman-Monteith formulation for calculating potential evapotranspiration
84 [*van der Schrier et al.*, 2013].

2.2. Climate Data

85 Monthly precipitation data used in the analyses are from the high-resolution CRU gridded
86 climate data [TS3.21, *Harris et al.*, 2014]. We also use monthly average indices from the
87 Climate Prediction Center from climate modes previously shown to have an influence on
88 Mediterranean climate [*Sousa et al.*, 2011]. The North Atlantic Oscillation [NAO; *Hurrell*,
89 1995] consists of a north-south dipole in atmospheric pressure between Greenland and the

subtropical North Atlantic, with positive phases typically associated with below-average precipitation in the Mediterranean and southern Europe. The Scandinavian Pattern [SCA; *Bueh and Nakamura, 2007*] is centered over Scandinavia, with positive height anomalies in this region causing above-average precipitation across central and southern Europe. The East Atlantic Pattern [EA; *Barnston and Livezey, 1987*] is similar to the NAO, consisting of a north-south anomaly dipole in the Atlantic. Unlike the NAO, however, the EA has stronger connections to the subtropical ridge. Positive phases of the EA are linked to below average precipitation across southern Europe. For the CRU precipitation data and the climate indices, we restrict our analysis for the most recent period when data quality and availability is highest (1950–2012).

2.3. Analyses

We use Spearman's rank correlations to assess the statistical relationship between reconstructions, observations, and indices. Spearman's is a non-parametric alternative to the Pearson product-moment correlation that is less sensitive to outliers. We also conduct spectral and spectral coherency analyses using a multi-taper approach [*Thomson, 1982; Chave et al., 1987; Mann and Lees, 1996; Czaja and Marshall, 2001; Huybers, 2004*] with significance levels estimated using a non-parametric Monte Carlo procedure with red noise (AR1) conditioned on the original data. Smoothing of time series by a 10-year lowess linear fit was applied to emphasize low frequency features in various time plots.

3. Results

3.1. Climate Signals in the OWDA

¹⁰⁸ Correlations between winter (January–March; JFM) and spring (April–June) precipitation and the tree-ring reconstructed JJA scPDSI are uniformly positive across the basin
¹⁰⁹ (Figure 2). The strongest correlations with JFM precipitation are localized in Spain and
¹¹⁰ Morocco in the western Mediterranean and the Levant region in the eastern basin. MAM
¹¹¹ precipitation correlations are more uniform and strongly positive across nearly the entire
¹¹² Mediterranean, suggesting that the summer season soil moisture variability, reflected in
¹¹³ the OWDA and the underlying tree growth, is driven primarily by spring precipitation
¹¹⁴ [c.f. *Touchan et al.*, 2014a].

¹¹⁶ Climate mode correlations with the CRU precipitation data or the OWDA scPDSI (Figure
¹¹⁷ 3) are consistent in sign, but generally stronger in the precipitation data. The weaker
¹¹⁸ OWDA scPDSI correlations are expected for at least two reasons. First, these climate
¹¹⁹ modes reflect shifts in atmospheric circulation that have a direct impact on precipitation
¹²⁰ by modulating, for example, storm track positions and moisture convergence. Circulation
¹²¹ impacts on the scPDSI will be by definition more indirect, as the scPDSI is computed
¹²² based on departures of a variety of variables from climatologically expected values (e.g.,
¹²³ soil moisture). Additionally, up to year 1978, the scPDSI is reconstructed as a scaled
¹²⁴ linear function of the underlying tree-ring proxies, meaning that (for this period) the cli-
¹²⁵ mate mode signal may be further obfuscated due to various biological processes (e.g., tree
¹²⁶ physiology, phenology, etc.).

¹²⁷ The influence of the NAO is strongest in winter and early spring (January–April;
¹²⁸ JFMA). Positive phases of the NAO cause drying across the northern reaches of the

¹²⁹ Mediterranean basin, from Spain and Morocco across to the Balkans and western Turkey,
¹³⁰ while favoring wetter conditions in coastal regions of Libya, Egypt, and the Levant. Con-
¹³¹ sistent with both the instrumental observations [e.g. *Lamb et al.*, 1997; *Knippertz et al.*,
¹³² 2003] and the underlying controls on tree growth [*Touchan et al.*, 2008a, b; *Panayotov
et al.*, 2010], the influence of the NAO in the OWDA is strongest in the far western part
¹³³ of the domain and the Balkans. The largest influence of the SCA pattern is during the
¹³⁴ winter (JFM), with positive phases increasing moisture across most of the basin. The SCA
¹³⁵ correlation with the OWDA is substantially weaker, consistent with previously analyses
¹³⁶ (Figure 2) demonstrating the much stronger connection between the OWDA and spring
¹³⁷ season, rather than winter, precipitation. Unlike the previous two modes, the influence of
¹³⁸ the EA is highest during the spring (AMJ), causing widespread drying across the basin
¹³⁹ with, notably, similar magnitude correlations with both precipitation and scPDSI.
¹⁴⁰

3.2. Drought Variability in the OWDA

¹⁴¹ Figure 4 shows OWDA scPDSI averaged over the Mediterranean domain and the fractional
¹⁴² land area in drought ($\text{scPDSI} \leq -1$) for each year from 1100–2012. Inter-annual variabil-
¹⁴³ ity (standard deviation) in the scPDSI is 0.54 standardized PDSI units and, on average,
¹⁴⁴ 29% of the basin experiences drought conditions in any given year. Highlighted are sev-
¹⁴⁵ eral example periods of persistent multi-year droughts and pluvials (Figure 4, grey bars).
¹⁴⁶ Noticeably absent are any extended multi-decadal (30-year or longer) ‘megadrought’ pe-
¹⁴⁷ riods, a characteristic feature of North American drought variability during the Medieval
¹⁴⁸ Climate Anomaly (approximately before 1300 CE) [e.g., *Cook et al.*, 2010] as well as
¹⁴⁹ previously inferred from Moroccan tree-rings [*Esper et al.*, 2007].

150 The spatial expression of the six highlighted periods of widespread drought (and one
151 pluvial) are shown in Figure 5. The most dramatic wet interval was a nearly two-decade
152 long period from 1125–1142 CE, with sustained wet conditions in modern day Spain,
153 Morocco, Algeria, Tunisia, Italy, the Balkans, and Turkey. Among the five highlighted
154 persistent drought events, there is a tendency for simultaneous drought in the extreme
155 western (Spain, Morocco, Algeria, Tunisia) and eastern (Balkans, Greece, Turkey) ends
156 of the basin. This is somewhat contrary to previous analyses of other proxy records in the
157 region, which have suggested instead a tendency for an anti-phased dipole in hydroclimate
158 variability between these two regions [e.g., *Roberts et al.*, 2012]. The basin-wide synchrony
159 found in these example events is further confirmed by compositing all years when at least
160 40% or 50% of the basin is in drought (Figure 6). Here, again, we can see the major poles
161 of synchronous and severe drought during these years of widespread drought are centered
162 over the opposite ends of the basin. In these events and composite, however, there is
163 some evidence for anti-phasing in the eastern end of the basin, where there is a tendency
164 for Libya, Egypt and the southern Levant to be wet or near normal when Greece and
165 Anatolia are in drought. This meridional dipole structure bears some resemblance to the
166 NAO correlation patterns with precipitation and scPDSI (Figure 3).

3.3. Spatial Synchrony

167 To further investigate the tendency for synchronous hydroclimate variability across the
168 basin, we averaged scPDSI from the OWDA over two regions: the western Mediterranean
169 (WestMED; 32°N–42°N, 10°W–0°E) and the eastern Mediterranean (EastMED; 36°N–
170 41°N, 20°E–37°E). The areas chosen for these regional indices correspond to approximately
171 the same areas used in the analysis of *Roberts et al.* [2012]. Point-by-point correlations

¹⁷² (Figure 7) between these two indices and the OWDA are strongly positive at the local
¹⁷³ level, as expected, decaying in magnitude outside of the averaging regions. For WestMED
¹⁷⁴ the correlations remain mostly positive, or near zero, across the entire basin, while the
¹⁷⁵ strong negative correlations with EastMED over Libya, Egypt, and the Levant provide
¹⁷⁶ further support for the existence of anti-phased hydroclimate behavior in these regions.
¹⁷⁷ Correlations between these indices and the opposite regions are only weakly positive,
¹⁷⁸ suggesting very weak coherency between WestMED and EastMED on inter-annual time
¹⁷⁹ scales.

¹⁸⁰ Frequency analyses of WestMED and EastMED show significant power in both series at
¹⁸¹ high (inter-annual) and low (decadal to multidecadal) frequencies (Figure 8). Both have
¹⁸² significant peaks at about 3–4 years, with EastMED additionally peaking at decadal fre-
¹⁸³ quencies and WestMED covering a broader range of multi-decadal bands. The two regions
¹⁸⁴ also overlap in their power at around 70 years, though EastMED is only marginally signif-
¹⁸⁵ icant at the 90th percentile. A coherency spectra analysis between the two regional indices
¹⁸⁶ demonstrates highly significant coherence between the two regions over inter-annual and
¹⁸⁷ decadal timescales (Figure 9). Notably, there is also a broad band of coherence between
¹⁸⁸ the two region at multi-decadal and centennial timescales (30 to 130 years), despite no
¹⁸⁹ significant spectral peaks at wavelengths longer than ~75 years in either WestMED or
¹⁹⁰ EastMED. This may be due to aliasing of shared frequencies: both series have peaks at
¹⁹¹ around 70-75 years, approximately the first harmonic of the 130 year coherence reflected
¹⁹² in the coherency spectra. Regardless, these results indicate that, at least over the last
¹⁹³ millennium, a reasonably strong tendency for in-phase drought across the Mediterranean,
¹⁹⁴ in sharp contrast to the inferences made by *Roberts et al.* [2012].

3.4. Recent Droughts

Recent decades have witnessed persistent, multi-year droughts in the Mediterranean that have spurred speculation that warming induced drying trends may have begun to emerge. In the OWDA, these droughts are not coherent across the Mediterranean basin but are, instead, highly localized in the WestMED region, Greece (36°N – 43°N , 19°E – 26°), and the Levant (30°N – 37°N , 33°E – 40°E) (Figure 10). Both WestMED and Greece experienced significant droughts in the 1980s and 1990s that have since ameliorated. The driest period in the Levant, by contrast, began in 1998, and has been generally ongoing since. Here, we attempt to place these most recent drought events within the context of OWDA drought variability for the last 900 years (Figure 11).

Over the last 30 years (1980–2012), we identify major periods of persistent drought in all three of these regions: 1980–2009 (WestMED), 1984–2002 (Greece), and 1998–2012 (Levant) (Figure 12, black dots). For each region, we then calculate the driest previous interval of the same length (Figure 12, grey dots). For both of these intervals, we estimate sampling uncertainties (the whiskers) using a Monte-Carlo procedure where we resample drought years from each interval with replacement, recalculating the mean scPDSI 10,000 times. The whiskers represent the 25th and 75th percentiles of these resampled means.

In general agreement with *Touchan et al.* [2008a], the recent persistent droughts in WestMED and Greece qualify as the most severe on the record. In both regions, however, there is substantial overlap in the uncertainties, and the recent droughts are not significantly drier (Student's t-test and Wilcoxon rank sum test, $p > 0.10$) than the previous driest intervals. From this, we conclude that, while severe, recent droughts in the

²¹⁶ WestMED region and Greece are not statistically separable from natural drought vari-
²¹⁷ ability over the last 900 years.

²¹⁸ The magnitude of the recent Levant drought also exceeds the magnitude of the driest
²¹⁹ previous interval in the region. In the Levant, mean scPDSI for 1998–2012 is -1.52 ,
²²⁰ compared to -1.1 for 1205–1219, with non-overlapping confidence limits between the two
²²¹ events. Despite this separation, 1998–2012 is not significantly drier than the previous
²²² driest period (One-Sided Student's t-test, $p = 0.13$). This is likely due to the leveraging
²²³ of the mean scPDSI for 1998–2012 by several extremely dry years: 1999 (scPDSI= -3.25),
²²⁴ 2000 (scPDSI= -4.49 , the driest single year in this region back to 1100), 2008 (scPDSI=
²²⁵ -2.80), and 2012 (scPDSI= -2.72). In our 89% of our Monte-Carlo simulations, however,
²²⁶ the resampled mean scPDSI for 1998–2012 was drier than the resampled mean for the
²²⁷ previous driest interval, 1205–1219. We therefore conclude that it is likely that 1998–2012
²²⁸ in the Levant was the driest 15-year period of the last 900 years, suggesting the possible
²²⁹ emergence of a greenhouse gas forced drying signal.

4. Discussion and Conclusions

²³⁰ Paleoclimate reconstructions provide better sampling of the full spectrum of natural vari-
²³¹ ability in the climate system, variability that is often not adequately captured by the
²³² relatively short instrumental record. This knowledge is especially critical for identifying
²³³ decadal and multidecadal variability and for evaluating the extent to which anthropogenic
²³⁴ forcing may be influencing recent climate trends and events. But while a variety of local
²³⁵ reconstruction efforts have been previously undertaken for the Mediterranean, field recon-
²³⁶ structions provide an opportunity to understand natural and anthropogenic patterns at
²³⁷ broader spatial and extended temporal scales.

238 Our analysis of the OWDA shows significant decadal to multi-decadal variability in
239 hydroclimate across the Mediterranean, with significant coherence between the western
240 and eastern basin centers on multi-decadal to centennial time scales. The dynamics driving
241 this synchrony are still uncertain, but the NAO or processes linked to the North Atlantic
242 are likely to be a major contributor to this pattern [*Hurrell and Loon, 1997; Eshel and*
243 *Farrell, 2000*]. The NAO mode is negatively correlated with precipitation and scPDSI
244 across the basin (Figure 2) and at the decadal scale is associated with same-sign wet
245 season (boreal winter) precipitation anomalies from Morocco and the Iberian Peninsula
246 though western and central Anatolia, with opposing anomalies in the Levant [*Mariotti*
247 *et al., 2002; Xoplaki et al., 2004*].

248 While there is a zonal dipole in the Mediterranean tree-ring response to precipitation,
249 with a stronger winter response to the west and an increasing spring-summer signal in
250 the east [*Touchan et al., 2014a, b*], at decadal timescales at least the summer scPDSI
251 does appear to reflect the broad-scale forcing of precipitation anomalies associated with
252 the NAO. This creates a basin-wide coherence between northwestern Africa, the Balkans,
253 and western Anatolia (Figure 9) and opposite sign anomalies in the Levant during major
254 Mediterranean drought and pluvial events (Figure 5–7).

255 Interestingly, this coherent decadal pattern is somewhat different than that observed
256 for recent scPDSI trends (Figure 10, 11), with the western Mediterranean and the Levant
257 experiencing more substantial drying trends, and with mixed signs over Anatolia. This
258 suggests that NAO variability alone may not account for recent drought trends, and
259 supports interpretations that greenhouse gas forcing has an important influence [*Kelley*
260 *et al., 2012, 2015; Seager et al., 2014*]. Although some climate model simulations suggest

²⁶¹ recent NAO trends are outside the range of natural variability [Osborn, 2004; Kuzmina
²⁶² et al., 2005], long control simulations can demonstrate unforced NAO variability similar
²⁶³ to that seen in recent decades [Semenov et al., 2008]. Drying in the Levant is also likely
²⁶⁴ influenced by recent trends toward a more positive EA pattern [Krichak et al., 2002;
²⁶⁵ Krichak and Alpert, 2005; Lim, 2014].

²⁶⁶ Our findings here suggest that, at least in the western Mediterranean and Anatolia,
²⁶⁷ the recent severe decadal-scale dry conditions are not yet outside the range of natural
²⁶⁸ variability, despite the influence of greenhouse gas forcing. In the Levant, however, we
²⁶⁹ estimate that the last 15 years are likely the driest since the 12th century. Drought
²⁷⁰ conditions here reduce water supply in the face of increasing demand, and create the
²⁷¹ potential for sociopolitical and economic disruption [e.g. Gleick, 2014; Kelley et al., 2015],
²⁷² requiring a multidisciplinary research, management, and policy approach [Sohl and van
²⁷³ Ginkel, 2014]. To that end, paleoclimate field reconstructions of drought can provide
²⁷⁴ valuable information on the long-term and broad-scale context of recent events, especially
²⁷⁵ how they fit within the context of natural climate variability.

²⁷⁶ **Acknowledgments.** Funding for Anchukaitis, Meko, and Toucan provided by NSF
²⁷⁷ Earth System History Grant #ESH0317288. Lamont contribution #.

References

²⁷⁸ Akkemik, U., and A. Aras (2005), Reconstruction (1689-1994 AD) of April-August pre-
²⁷⁹ cipitation in the southern part of central Turkey, *International Journal of Climatology*,
²⁸⁰ 25(4), 537–548, doi:10.1002/joc.1145.

- 281 Andreu, L., E. Gutiérrez, M. Macias, M. Ribas, O. Bosch, and J. J. Camarero (2007),
282 Climate increases regional tree-growth variability in Iberian pine forests, *Global Change
Biology*, 13(4), 804–815, doi:DOI:10.1111/j.1365-2486.2007.01322.x.
- 284 Barnston, A. G., and R. E. Livezey (1987), Classification, Seasonality and Persistence
285 of Low-Frequency Atmospheric Circulation Patterns, *Monthly Weather Review*, 115(6),
286 1083–1126, doi:10.1175/1520-0493(1987)115<1083:CSAPOL>2.0.CO;2.
- 287 Bueh, C., and H. Nakamura (2007), Scandinavian pattern and its climatic impact,
288 *Quarterly Journal of the Royal Meteorological Society*, 133(629), 2117–2131, doi:
289 DOI:10.1002/qj.173.
- 290 Büntgen, U., D. Frank, V. Trouet, and J. Esper (2010), Diverse climate sensitivity
291 of Mediterranean tree-ring width and density, *Trees*, 24(2), 261–273, doi:10.1007/
292 s00468-009-0396-y.
- 293 Chave, A. D., D. J. Thomson, and M. E. Ander (1987), On the robust estimation of
294 power spectra, coherences, and transfer functions, *Journal of Geophysical Research:
Atmospheres*, 92(B1), 633, doi:10.1029/jb092ib01p00633.
- 296 Chbouki, N., C. W. Stockton, and D. Myers (1995), Spatio-temporal patterns of drought
297 in Morocco, *International Journal of Climatology*, 15, 187–205, doi:DOI:10.1002/joc.
298 3370150205.
- 299 Cook, E. R., R. Seager, R. R. Heim Jr, R. S. Vose, C. Herweijer, and C. Woodhouse
300 (2010), Megadroughts in North America: placing IPCC projections of hydroclimatic
301 change in a long-term palaeoclimate context, *Journal of Quaternary Science*, 25(1),
302 48–61, doi:10.1002/jqs.1303.

- 303 Cook, E. R., R. Seager, Y. Kushnir, K. R. Briffa, U. Büntgen, D. Frank, P. J. Krusic,
304 et al. (in review), Old World Droughts and Pluvials During the Common Era, *Science*.
305 Czaja, A., and J. Marshall (2001), Observations of atmosphere-ocean coupling in the
306 north atlantic, *Q.J Royal Met. Soc.*, 127(576), 1893–1916, doi:10.1002/qj.49712757603.
307 Eshel, G., and B. F. Farrell (2000), Mechanisms of eastern Mediterranean rainfall vari-
308 ability, *Journal of the Atmospheric Sciences*, 57(19), 3219–3232.
309 Esper, J., D. Frank, U. Büntgen, A. Verstege, J. Luterbacher, and E. Xoplaki (2007), Long-
310 term drought severity variations in Morocco, *Geophysical Research Letters*, 34(17),
311 L17702, doi:10.1029/2007GL030844.
312 García-Ruiz, J. M., J. I. López-Moreno, S. M. Vicente-Serrano, T. Lasanta-Martínez, and
313 S. Beguería (2011), Mediterranean water resources in a global change scenario, *Earth-
314 Science Reviews*, 105(3–4), 121 – 139, doi:[http://dx.doi.org/10.1016/j.earscirev.2011.
315 01.006](http://dx.doi.org/10.1016/j.earscirev.2011.01.006).
316 Giorgi, F., and P. Lionello (2008), Climate change projections for the Mediterranean
317 region, *Global and Planetary Change*, 63(2–3), 90 – 104, doi:<http://dx.doi.org/10.1016/j.gloplacha.2007.09.005>, mediterranean climate: trends, variability and change.
318 Gleick, P. H. (2014), Water, Drought, Climate Change, and Conflict in Syria, *Weather,
319 Climate, and Society*, 6(3), 331–340, doi:10.1175/WCAS-D-13-00059.1.
320 Glueck, M. F., and C. W. Stockton (2001), Reconstruction of the North Atlantic Os-
321 cillation, 1429–1983, *International Journal of Climatology*, 21, 1453–1465, doi:DOI:
322 10.1002/joc.684.
323 Guttman, N. B. (1998), Comparing the Palmer Drought Index and the Standardized
324 Precipitation Index, *Journal of the American Water Resources Association*, 34, 113–

- 326 121, doi:10.1111/j.1752-1688.1998.tb05964.x.
- 327 Harris, I., P. D. Jones, T. J. Osborn, and D. H. Lister (2014), Updated high-resolution
328 grids of monthly climatic observations –the CRU TS3.10 Dataset, *International Journal
329 of Climatology*, 34(3), 623–642, doi:10.1002/joc.3711.
- 330 Held, I. M., and B. J. Soden (2006), Robust Responses of the Hydrological Cycle to
331 Global Warming, *Journal of Climate*, 19(21), 5686–5699, doi:[http://dx.doi.org/10.
332 1175/JCLI3990.1](http://dx.doi.org/10.1175/JCLI3990.1).
- 333 Hoerling, M., J. Eischeid, J. Perlwitz, X. Quan, T. Zhang, and P. Pegion (2012), On the
334 Increased Frequency of Mediterranean Drought, *Journal of Climate*, 25(6), 2146–2161,
335 doi:10.1175/JCLI-D-11-00296.1.
- 336 Hurrell, J. W. (1995), Decadal Trends in the North Atlantic Oscillation: Regional Tem-
337 peratures and Precipitation, *Science*, 269(5224), 676–679, doi:10.1126/science.269.5224.
338 676.
- 339 Hurrell, J. W., and H. V. Loon (1997), Decadal Variations in Climate Associated with
340 the North Atlantic Oscillation, in *Climatic Change at High Elevation Sites*, pp. 69–94,
341 Springer Netherlands, doi:10.1007/978-94-015-8905-5_4.
- 342 Huybers, P. (2004), Comments on ‘coupling of the hemispheres in observations and sim-
343 ulations of glacial climate change’ by a. schmittner, o.a. saenko, and a.j. weaver’, *Qua-*
344 *ternary Science Reviews*, 23(1-2), 207–210, doi:10.1016/j.quascirev.2003.08.001.
- 345 Iglesias, A., L. Garrote, F. Flores, and M. Moneo (2007), Challenges to Manage the
346 Risk of Water Scarcity and Climate Change in the Mediterranean, *Water Resources
347 Management*, 21(5), 775–788, doi:10.1007/s11269-006-9111-6.

- ³⁴⁸ Jex, C. N., A. Baker, J. M. Eden, W. J. Eastwood, I. J. Fairchild, M. J. Leng, L. Thomas,
³⁴⁹ and H. J. Sloane (2011), A 500 yr speleothem-derived reconstruction of late autumn–
³⁵⁰ winter precipitation, northeast Turkey, *Quaternary Research*, 75(3), 399–405, doi:
³⁵¹ DOI:10.1016/j.yqres.2011.01.005.
- ³⁵² Jones, M. D., C. N. Roberts, M. J. Leng, and M. Türkeş (2006), A high-resolution late
³⁵³ Holocene lake isotope record from Turkey and links to North Atlantic and monsoon
³⁵⁴ climate, *Geology*, 34(5), 361–364, doi:doi:10.1130/G22407.1.
- ³⁵⁵ Kelley, C., M. Ting, R. Seager, and Y. Kushnir (2012), The relative contributions
³⁵⁶ of radiative forcing and internal climate variability to the late 20th Century win-
³⁵⁷ ter drying of the Mediterranean region, *Climate Dynamics*, 38(9-10), 2001–2015, doi:
³⁵⁸ 10.1007/s00382-011-1221-z.
- ³⁵⁹ Kelley, C. P., S. Mohtadi, M. A. Cane, R. Seager, and Y. Kushnir (2015), Climate change
³⁶⁰ in the Fertile Crescent and implications of the recent Syrian drought, *Proceedings of the
361 National Academy of Sciences*, 112(11), 3241–3246, doi:10.1073/pnas.1421533112.
- ³⁶² Knippertz, P., M. Christoph, and P. Speth (2003), Long-term precipitation variability
³⁶³ in Morocco and the link to the large-scale circulation in recent and future climates,
³⁶⁴ *Meteorology and Atmospheric Physics*, 83(1), 67–88, doi:10.1007/s00703-002-0561-y.
- ³⁶⁵ Köse, N., U. Akkemik, H. N. Dalfes, and M. S. Özeren (2011), Tree-ring reconstructions
³⁶⁶ of May–June precipitation for western Anatolia, *Quaternary Research*, 75(3), 438–450,
³⁶⁷ doi:10.1016/j.yqres.2010.12.005.
- ³⁶⁸ Krichak, S., P. Kishcha, and P. Alpert (2002), Decadal trends of main Eurasian oscilla-
³⁶⁹ tions and the Eastern Mediterranean precipitation, *Theoretical and Applied Climatology*,
³⁷⁰ 72(3-4), 209–220.

- ³⁷¹ Krichak, S. O., and P. Alpert (2005), Decadal trends in the east Atlantic–west Russia
³⁷² pattern and Mediterranean precipitation, *International Journal of Climatology*, 25(2),
³⁷³ 183–192, doi:10.1002/joc.1124.
- ³⁷⁴ Kuzmina, S. I., L. Bengtsson, O. M. Johannessen, H. Drange, L. P. Bobylev, and M. W.
³⁷⁵ Miles (2005), The North Atlantic Oscillation and greenhouse-gas forcing, *Geophysical*
³⁷⁶ *Research Letters*, 32(4), doi:10.1029/2004gl021064.
- ³⁷⁷ Lamb, P. J., , M. E. Hamly, and D. H. Portis (1997), North Atlantic Oscillation, *Geo*
³⁷⁸ *Observateur*, 7, 103–113.
- ³⁷⁹ Lim, Y.-K. (2014), The East Atlantic/West Russia (EA/WR) teleconnection in the North
³⁸⁰ Atlantic: climate impact and relation to Rossby wave propagation, *Climate Dynamics*,
³⁸¹ doi:10.1007/s00382-014-2381-4.
- ³⁸² Mann, M. E., and J. M. Lees (1996), Robust estimation of background noise and signal de-
³⁸³ tection in climatic time series, *Clim. Change*, 33(3), 409–445, doi:10.1007/BF00142586.
- ³⁸⁴ Mariotti, A., M. V. Struglia, N. Zeng, and K. Lau (2002), The hydrological cycle in the
³⁸⁵ Mediterranean region and implications for the water budget of the Mediterranean Sea,
³⁸⁶ *Journal of climate*, 15(13), 1674–1690, doi:[http://dx.doi.org/10.1175/1520-0442\(2002\)015<1674:THCITM>2.0.CO;2](http://dx.doi.org/10.1175/1520-0442(2002)015<1674:THCITM>2.0.CO;2).
- ³⁸⁷ Moreno, A., A. Pérez, J. Frigola, V. Nieto-Moreno, M. Rodrigo-Gámiz, B. Martrat,
³⁸⁸ P. González-Sampériz, M. Morellón, C. Martín-Puertas, J. P. Corella, et al. (2012),
³⁸⁹ The Medieval Climate Anomaly in the Iberian Peninsula reconstructed from marine
³⁹⁰ and lake records, *Quaternary Science Reviews*, 43, 16–32, doi:DOI:10.1016/j.quascirev.
³⁹¹ 2012.04.007.

- 393 Nicault, A., S. Alleaume, S. Brewer, M. Carrer, P. Nola, and J. Guiot (2008), Mediterranean
394 drought fluctuation during the last 500 years based on tree-ring data, *Climate
395 Dynamics*, 31(2-3), 227–245, doi:10.1007/s00382-007-0349-3.
- 396 Osborn, T. (2004), Simulating the winter North Atlantic Oscillation: the roles of inter-
397 internal variability and greenhouse gas forcing, *Climate Dynamics*, 22(6-7), doi:10.1007/
398 s00382-004-0405-1.
- 399 Palmer, W. C. (1965), Meteorological drought, *Tech. rep.*, US Weather Bureau, Wash-
400 ton, DC.
- 401 Panayotov, M., P. Bebi, V. Trouet, and S. Yurukov (2010), Climate signal in tree-ring
402 chronologies of Pinus peuce and Pinus heldreichii from the Pirin Mountains in Bulgaria,
403 *Trees*, 24(3), 479–490, doi:10.1007/s00468-010-0416-y.
- 404 Roberts, N., A. Moreno, B. L. Valero-Garcés, J. P. Corella, M. Jones, S. Allcock, J. Wood-
405 bridge, M. Morellón, J. Luterbacher, E. Xoplaki, et al. (2012), Palaeolimnological evi-
406 dence for an east–west climate see-saw in the Mediterranean since AD 900, *Global and
407 Planetary Change*, 84, 23–34, doi:DOI:10.1016/j.gloplacha.2011.11.002.
- 408 Seager, R., N. Naik, and G. A. Vecchi (2010), Thermodynamic and Dynamic Mechanisms
409 for Large-Scale Changes in the Hydrological Cycle in Response to Global Warming,
410 *Journal of Climate*, 23(17), 4651–4668, doi:10.1175/2010JCLI3655.1.
- 411 Seager, R., H. Liu, N. Henderson, I. Simpson, C. Kelley, T. Shaw, Y. Kushnir, and
412 M. Ting (2014), Causes of Increasing Aridification of the Mediterranean Region in
413 Response to Rising Greenhouse Gases, *Journal of Climate*, 27(12), 4655–4676, doi:
414 10.1175/JCLI-D-13-00446.1.

- 415 Seim, A., K. Treydte, V. Trouet, D. Frank, P. Fonti, W. Tegel, M. Panayotov,
416 L. Fernández-Donado, P. Krusic, and U. Büntgen (2014), Climate sensitivity of Mediter-
417 ranean pine growth reveals distinct east–west dipole, *International Journal of Clima-*
418 *tology, Early View*, doi:10.1002/joc.4137.
- 419 Semenov, V. A., M. Latif, J. H. Jungclaus, and W. Park (2008), Is the observed NAO vari-
420 ability during the instrumental record unusual?, *Geophysical Research Letters*, 35(11),
421 doi:10.1029/2008gl033273.
- 422 Sohl, M., and M. van Ginkel (2014), Drought preparedness and drought mitigation in the
423 developing worlds drylands, *Weather and Climate Extremes*, 3, 62 – 66, doi:<http://dx.doi.org/10.1016/j.wace.2014.03.003>, high Level Meeting on National Drought Policy.
- 425 Sousa, P. M., R. M. Trigo, P. Aizpurua, R. Nieto, L. Gimeno, R. Garcia-Herrera, P. Li-
426 onello, and M. Maugeri (2011), Trends and extremes of drought indices throughout the
427 20th century in the Mediterranean, *Natural Hazards & Earth System Sciences*, 11(1),
428 33 – 51, doi:doi:10.5194/nhess-11-33-2011.
- 429 Thomson, D. J. (1982), Spectrum estimation and harmonic analysis, *Proceedings of the
430 IEEE*, 70, 1055–1096.
- 431 Touchan, R., G. M. Garfin, D. M. Meko, G. Funkhouser, N. Erkan, M. K. Hughes, and
432 B. S. Wallin (2003), Preliminary reconstructions of spring precipitation in southwestern
433 Turkey from tree-ring width, *International Journal of Climatology*, 23(2), 157–171, doi:
434 DOI:10.1002/joc.850.
- 435 Touchan, R., E. Xoplaki, G. Funkhouser, J. Luterbacher, M. K. Hughes, N. Erkan,
436 U. Akkemik, and J. Stephan (2005), Reconstructions of spring/summer precipitation for
437 the Eastern Mediterranean from tree-ring widths and its connection to large-scale atmo-

- 438 spheric circulation, *Climate Dynamics*, 25(1), 75–98, doi:10.1007/s00382-005-0016-5.
- 439 Touchan, R., K. J. Anchukaitis, D. M. Meko, S. Attalah, C. Baisan, and A. Aloui (2008a),
440 Long term context for recent drought in northwestern Africa, *Geophysical Research
Letters*, 35(13), L13,705, doi:DOI:10.1029/2008GL034264.
- 441 Touchan, R., D. Meko, and A. Aloui (2008b), Precipitation reconstruction for North-
442 western Tunisia from tree rings, *Journal of Arid Environments*, 72(10), 1887–1896,
443 doi:10.1016/j.jaridenv.2008.05.010.
- 444 Touchan, R., K. J. Anchukaitis, D. M. Meko, M. Sabir, S. Attalah, and A. Aloui (2011),
445 Spatiotemporal drought variability in northwestern Africa over the last nine centuries,
446 *Climate Dynamics*, 37(1–2), 237–252, doi:10.1007/s00382-010-0804-4.
- 447 Touchan, R., K. J. Anchukaitis, V. V. Shishov, F. Sivrikaya, J. Attieh, M. Ketmen,
448 J. Stephan, I. Mitsopoulos, A. Christou, and D. M. Meko (2014a), Spatial Patterns of
449 eastern Mediterranean climate influence on tree growth, *The Holocene*, 24(4), 381–392,
450 doi:10.1177/0959683613518594.
- 451 Touchan, R., D. M. Meko, and K. J. Anchukaitis (2014b), Dendroclimatology in the
452 Eastern Mediterranean, *Tree-Ring Research*, *in press*.
- 453 van der Schrier, G., J. Barichivich, K. R. Briffa, and P. D. Jones (2013), A scPDSI-based
454 global data set of dry and wet spells for 1901–2009, *Journal of Geophysical Research:
455 Atmospheres*, doi:10.1002/jgrd.50355.
- 456 Vicente-Serrano, S. M., S. Beguería, J. I. López-Moreno, M. Angulo, and A. El Kenawy
457 (2010), A new global 0.5 gridded dataset (1901-2006) of a multiscalar drought index:
458 comparison with current drought index datasets based on the Palmer Drought Severity
459 Index, *Journal of Hydrometeorology*, 11(4), 1033–1043, doi:<http://dx.doi.org/10.1175/>
- 460

461 2010JHM1224.1.

462 Wassenburg, J. A., A. Immenhauser, D. K. Richter, A. Niedermayr, S. Riechelmann,

463 J. Fietzke, D. Scholz, K. P. Jochum, J. Fohlmeister, A. Schröder-Ritzrau, et al. (2013),

464 Moroccan speleothem and tree ring records suggest a variable positive state of the North

465 Atlantic Oscillation during the Medieval Warm Period, *Earth and Planetary Science*

466 *Letters*, 375, 291–302, doi:DOI:10.1016/j.epsl.2013.05.048.

467 Xoplaki, E., J. González-Rouco, J. Luterbacher, and H. Wanner (2004), Wet season

468 Mediterranean precipitation variability: influence of large-scale dynamics and trends,

469 *Climate Dynamics*, 23(1), doi:10.1007/s00382-004-0422-0.

Tree–Ring Chronologies

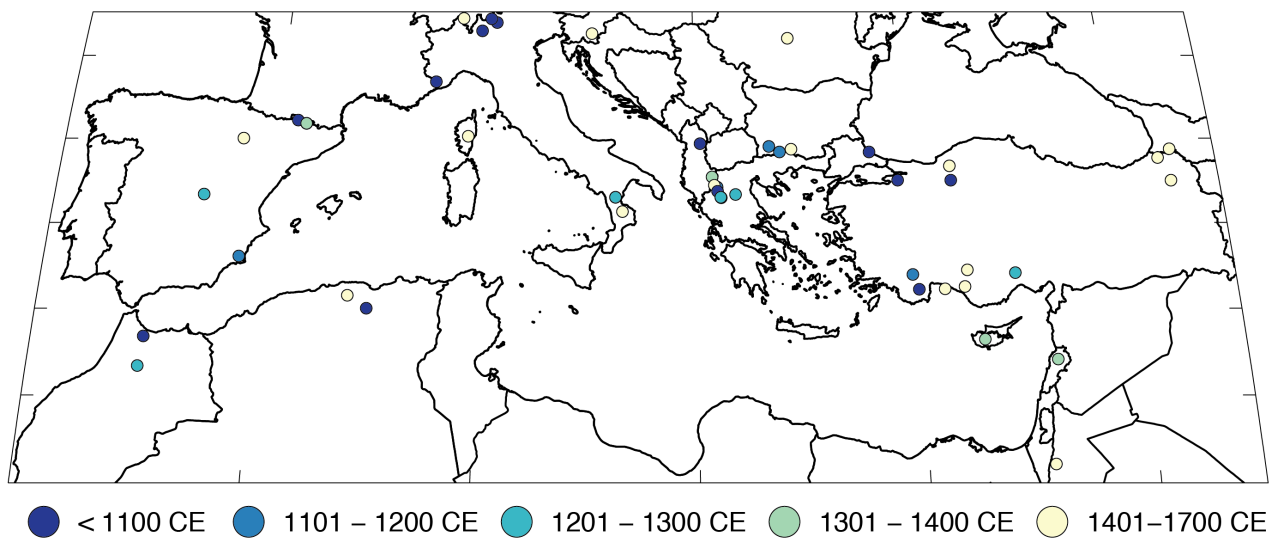


Figure 1. Locations of tree-ring chronologies used for the Mediterranean portion of the Old World Drought Atlas. Colors indicate the start dates of the various chronologies.

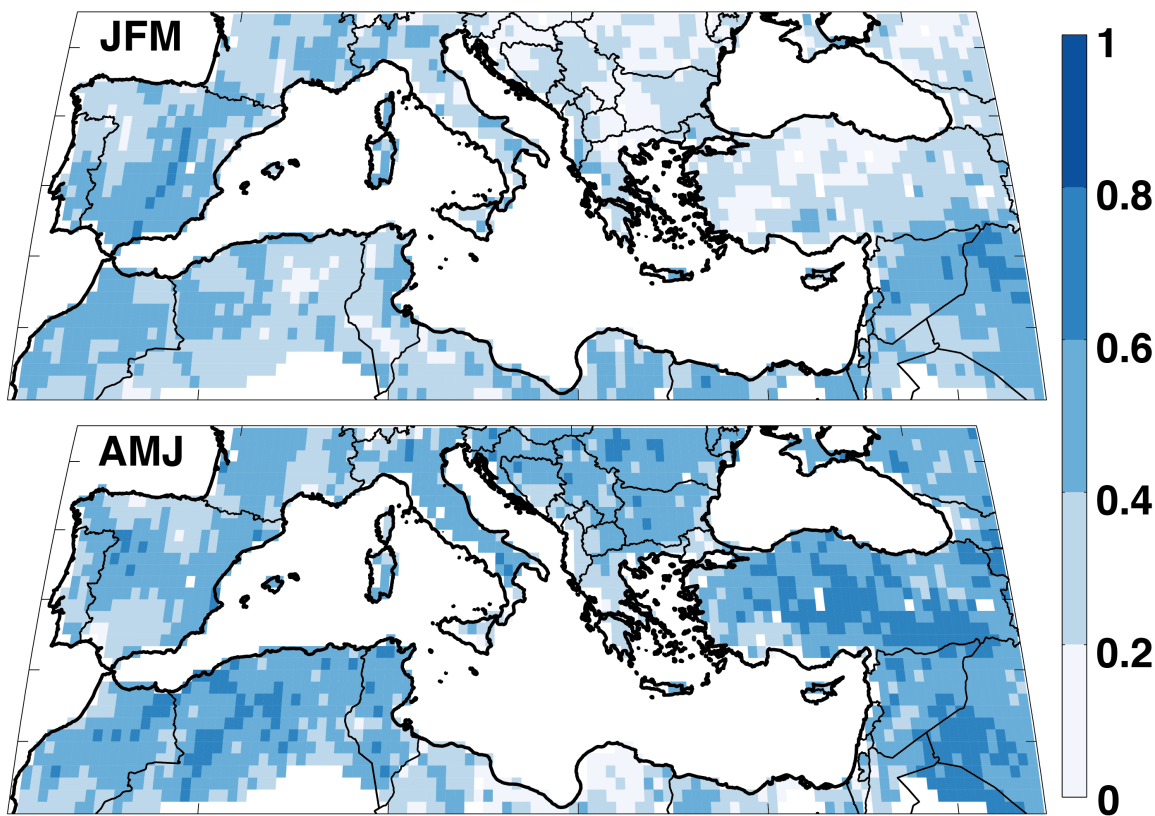


Figure 2. Point-by-point Spearman's rank correlation coefficients between CRU 3.21 pre-
cipitation totals (JFM and AMJ) and OWDA summer season (JJA) scPDSI. Correlations are
calculated over the period 1950–2012 CE.

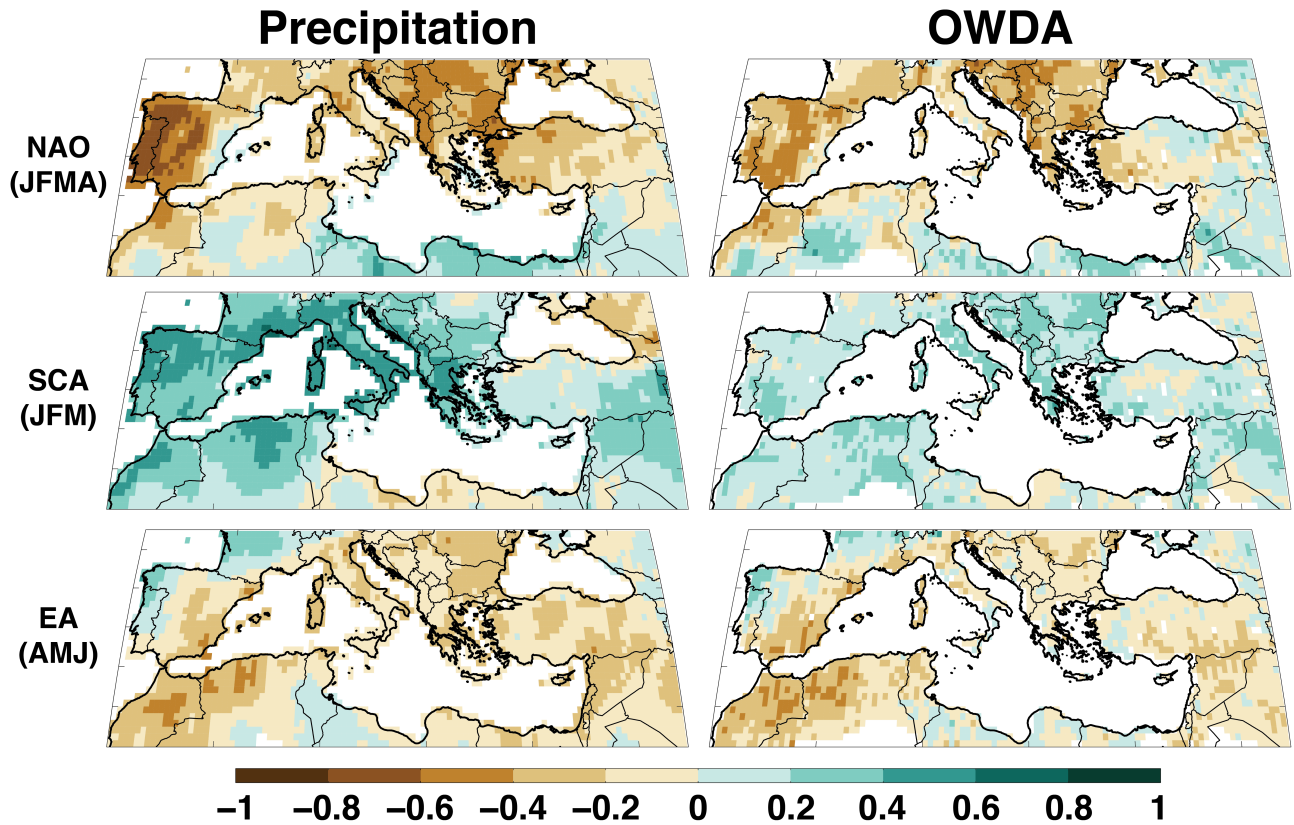


Figure 3. Spearman's rank correlation coefficients between the teleconnection indices (NAO, SCA, EA) and simultaneous season CRU 3.21 precipitation totals (left column) and OWDA summer season scPDSI (right column). Correlations are calculated over the period 1950–2012 CE.

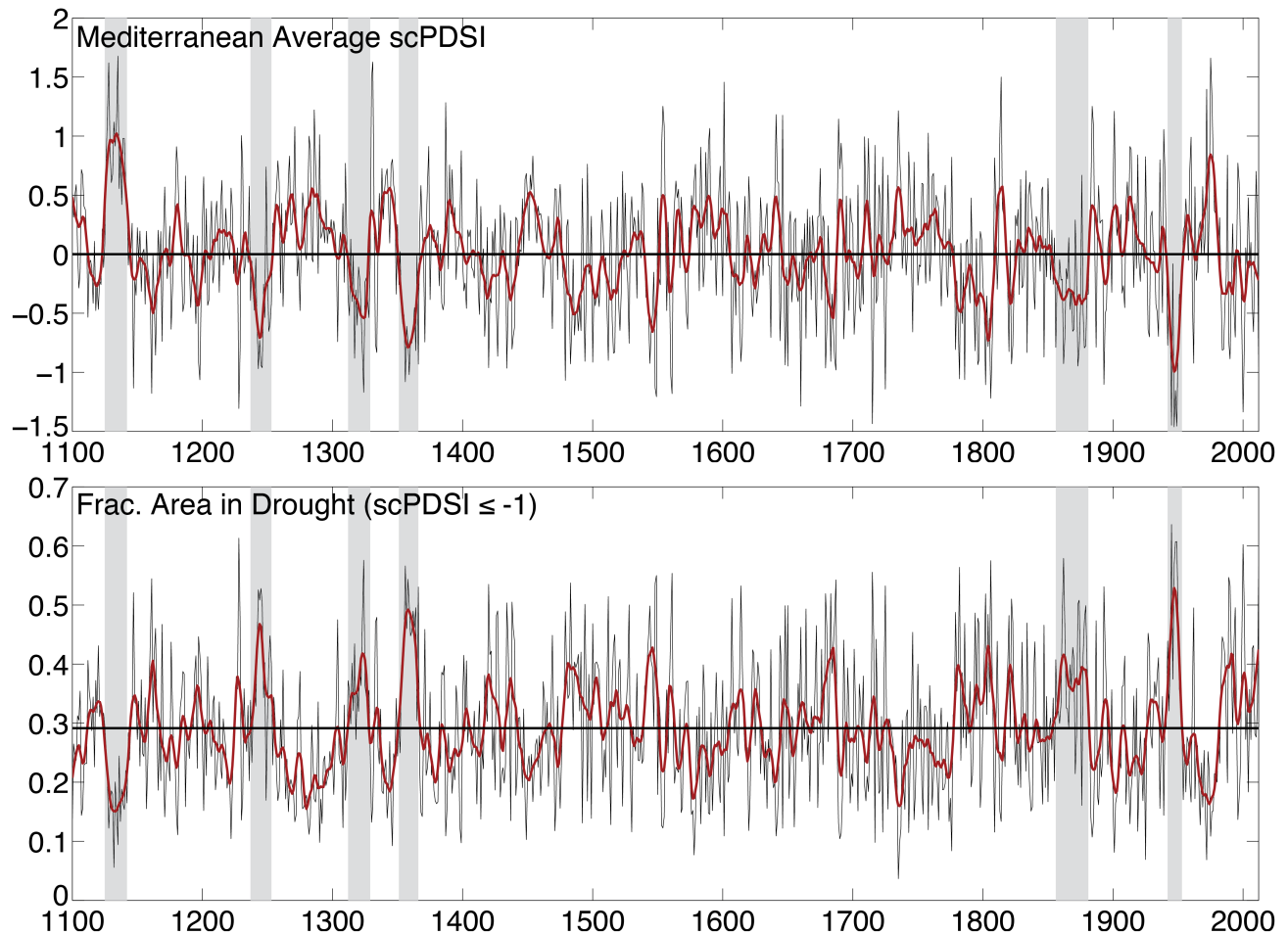


Figure 4. Area average scPDSI for the entire Mediterranean domain in the OWDA (30°N – 47°N , 10°W – 45°E) (top) and percent land area in drought ($\text{scPDSI} \leq -1$) (bottom) from 1100–2012 CE. Red curves are smoothed versions of the time series using a 10-year loess spline. The horizontal line in the lower panel is the long-term average fractional area in drought from 1100–2012 CE (29%). Highlighted in grey are several example period of persistent pan-basin drought and pluvial events (see Figure 5).

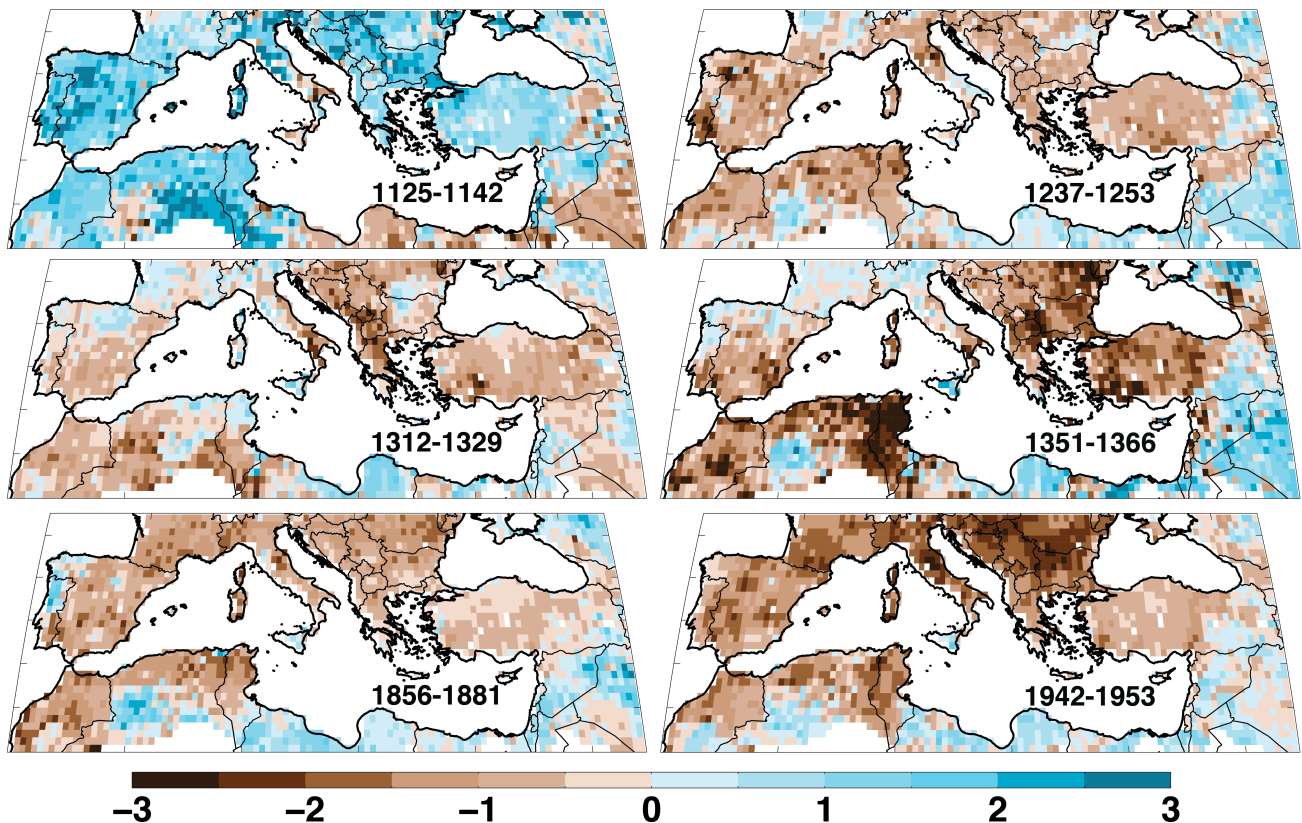


Figure 5. Multi-year average scPDSI for different pan-basin drought and pluvial events in the OWDA.

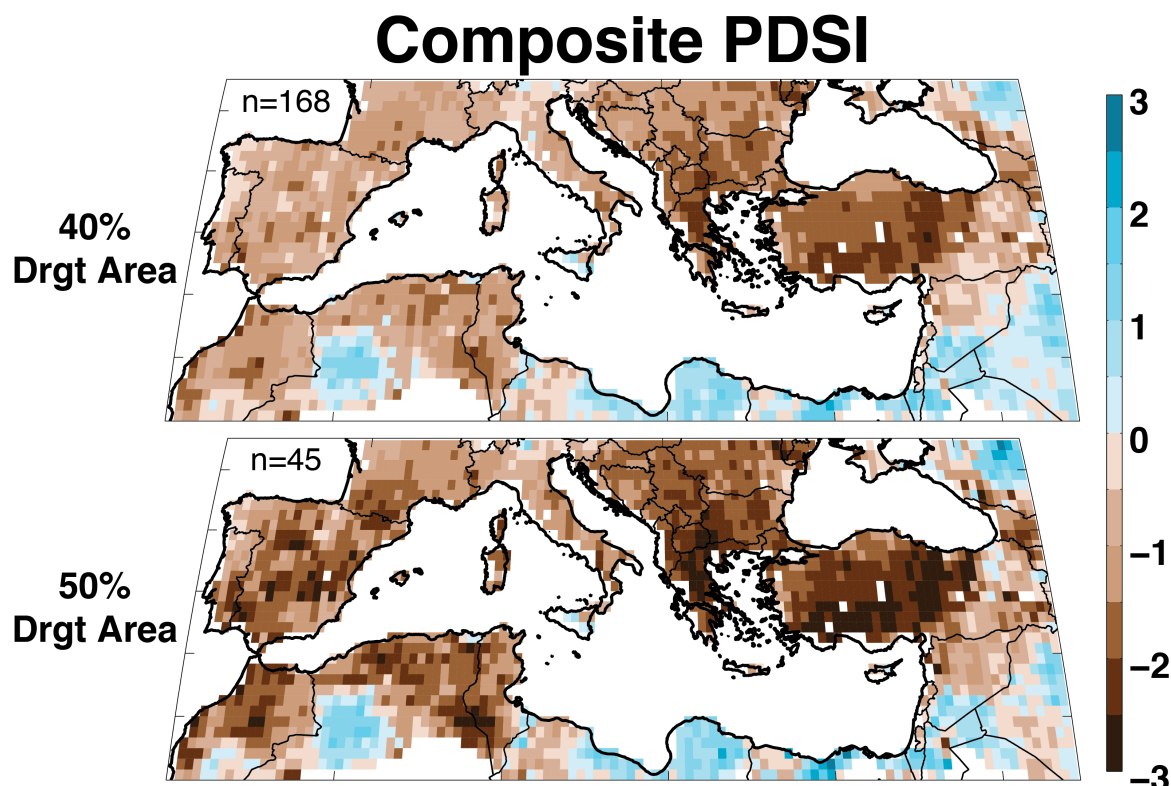


Figure 6. Composite average of Mediterranean drought events in the OWDA with a drought area ($\text{scPDSI} \leq -1$) exceeding 40% ($n = 168$ years) and 50% ($n = 45$ years) of the total land area in the Mediterranean domain.

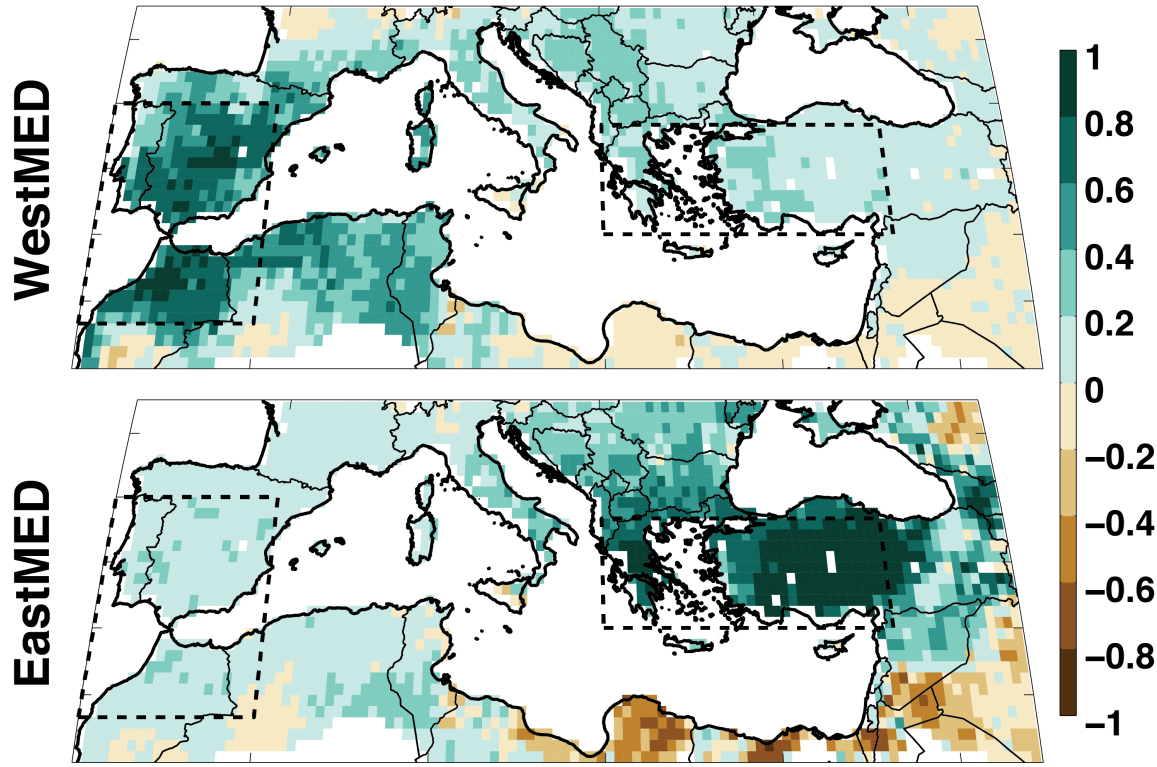


Figure 7. Point-by-point Spearman's rank correlations (1100–2012) between OWDA scPDSI and the Western Mediterranean (WestMED; 32°N–42°N, 10°W–0°) and Eastern Mediterranean (EastMED; 36°N–41°N, 20°E–37°E) regional average scPDSI time series.

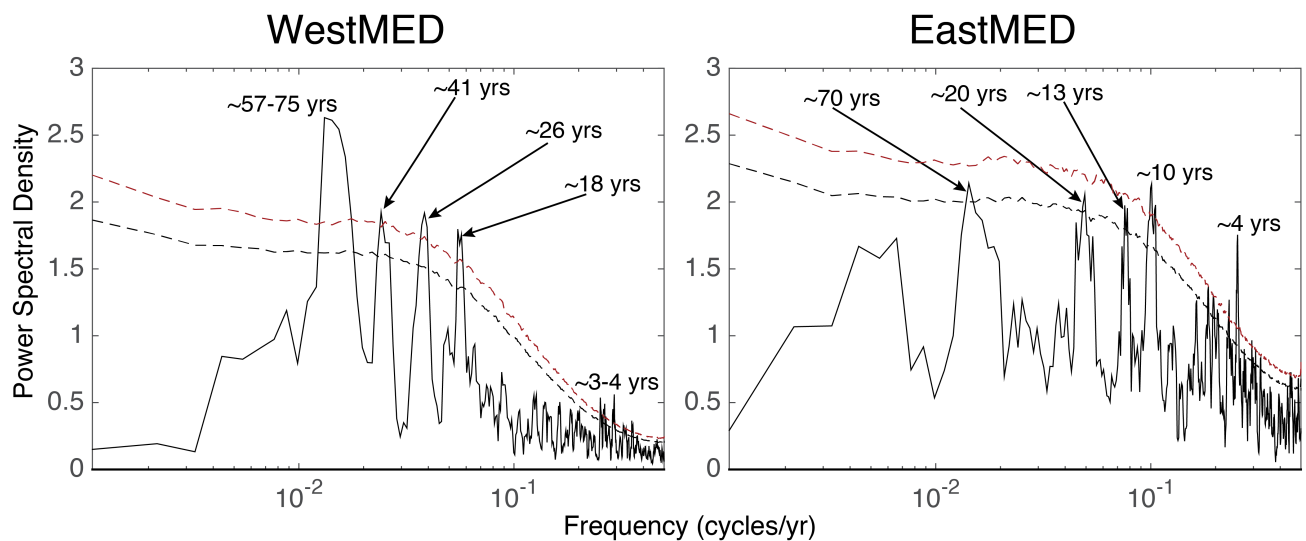


Figure 8. Power spectral density (Multi-taper Method, 3 tapers) for the WestMED and EastMED regional average scPDSI series. Red and black dashed lines are the 95th and 90th confidence limits, respectively, estimated from 10,000 AR(1) series generated from the original time series.

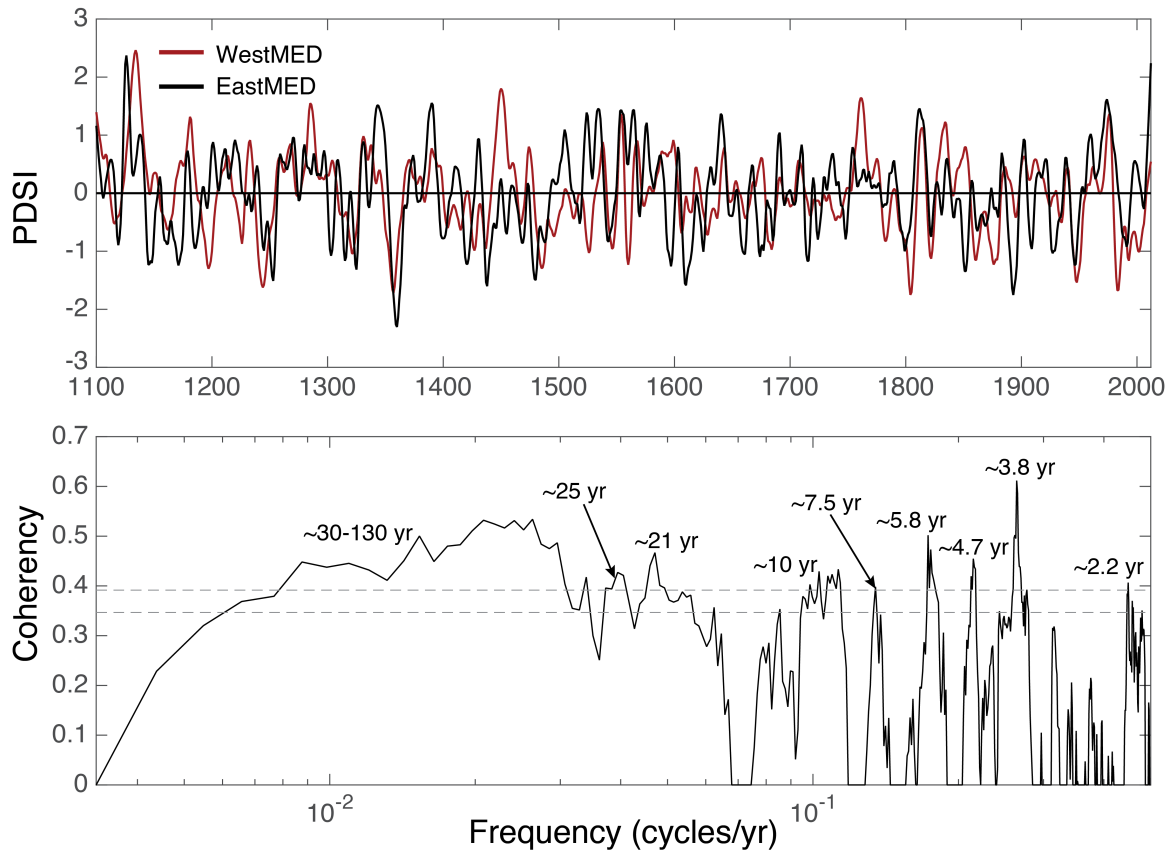


Figure 9. Smoothed versions (10-year loess spline) of the WestMED and EastMED time series (top) and the coherency spectra between the two unsmoothed series (bottom).

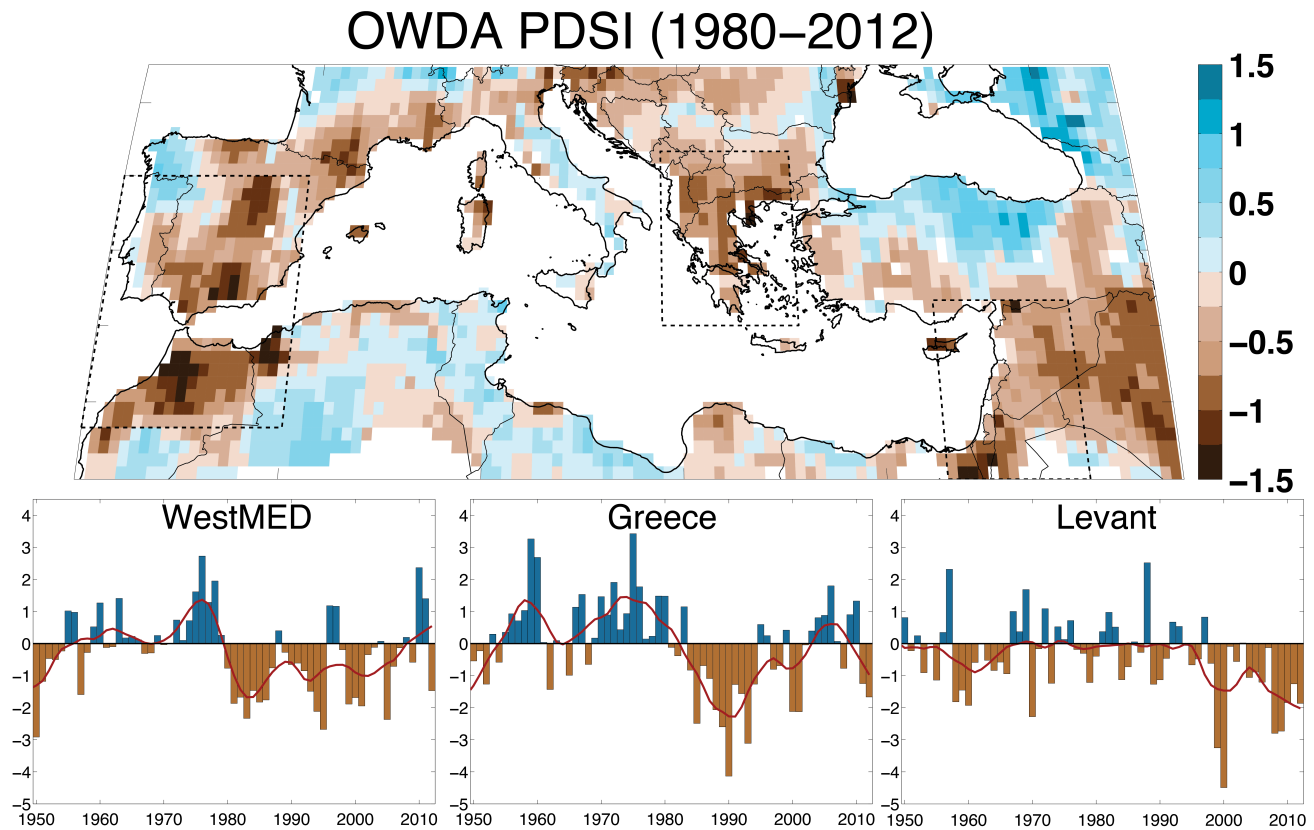


Figure 10. Multi-year average scPDSI for 1980–2012 (top) with regions of recent and persistent drought outlined in dashed black lines: WestMED (32°N – 42°N , 10°W – 0°), Greece (36°N – 43°N , 19°E – 26°), and the Levant (30°N – 37°N , 33°E – 40°E). Also shown (bottom) are the regional average scPDSI time series from these regions for 1950–2012 (red line is a 10-year loess smoother).

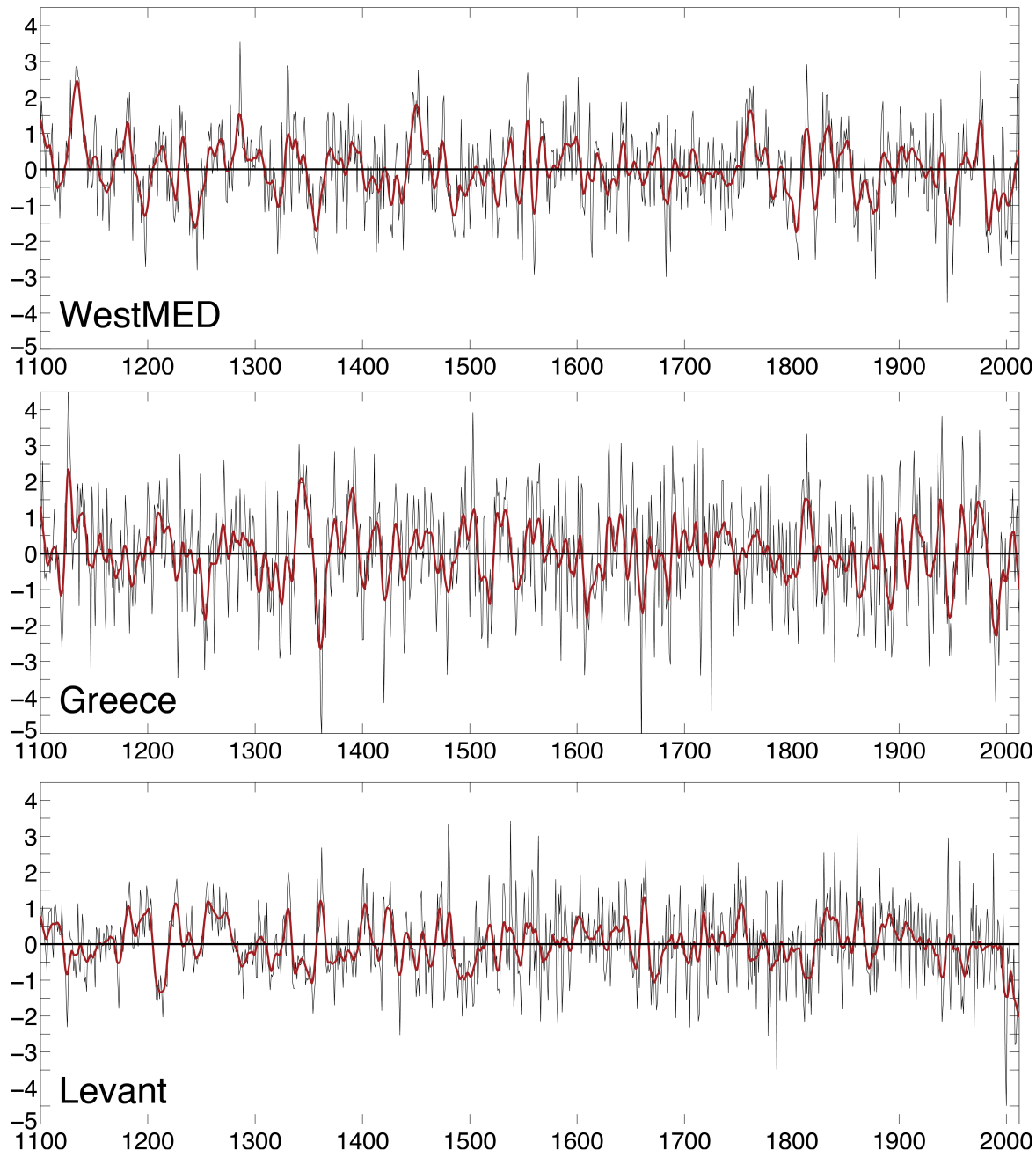


Figure 11. Re-centered (zero mean from 1100–2012 CE) time series for WestMED, Greece, and the Levant region. Red lines represent smoothed versions using a 10-year loess smoother.

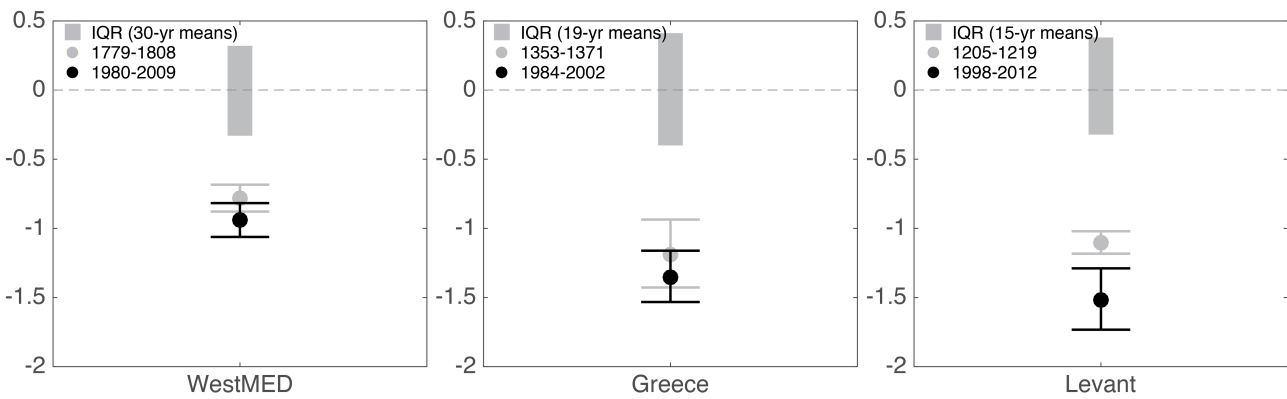


Figure 12. Comparisons between multi-year average re-centered scPDSI during recent decades (black dots) and driest previous periods of the same length in the OWDA from 1100–2012 CE. Grey bars are the interquartile range of mean PDSI for all such periods, grey dots represent the driest period prior to the recent decades, and black dots are the mean PDSI for the most recent drought. Whiskers are the 25th and 75th confidence limits for the dry events, estimated from 10,000 resamplings with replacement from scPDSI values during these intervals.